RSC Advances

PAPER

View Article Online
View Journal | View Issue

Cite this: *RSC Adv.*, 2020, **10**, 37463

Hydroxychalcone dyes that serve as color indicators for pH and fluoride ions†

Yanqing Du,[a] Fengying Liang,[a] Mixia Hu,[a] Ren Bu,[a] Meiling Wang,[a] Akihiko Tsuda *[ab] and Chaolu Eerdun *[a]

Received 4th August 2020
Accepted 3rd October 2020

DOI: 10.1039/d0ra06719a

rsc.li/rsc-advances

A chalcone, which is composed of two aromatic rings bridged by an α,β-unsaturated carbonyl group, exhibits a variety of biological activities. With an objective to develop a novel chalcone-based functional dye, we have synthesized a chalcone diol CLN**1**, bearing two OH groups at the 2-positions on both phenyl rings, as well as reference compounds CLN**2**–**6**, and found that it serves as color indicators for pH and fluoride ions. CLN**1** showed a vivid color change from colorless to yellow (halochromism) in water at pH ≥ 10. Furthermore, it presented a selective color change from colorless to red upon the addition of TBAF in an organic solvent such as CH_3CN. CLN**1** provided a strong red-shifted absorption band in the visible region under alkaline conditions in water and upon the addition of TBAF in CH_3CN. The absorption spectral study together with TD-DFT calculations and X-ray crystallographic analysis revealed that the characteristic π-resonant structures of CLN**1** caused by the ionization or OH–F^- interactions and the planar conformation due to its intramolecular hydrogen bonding may provide a strong charge transfer (CT) absorption in the visible region.

Introduction

A chalcone is widely distributed in plants such as vegetables, fruits, and teas.[1–4] It contains a unique α,β-unsaturated ketone structure with two aromatic rings (Chart 1), and exhibits a wide range of biological activities, such as anti-cancer, anti-inflammatory, antibacterial, and antioxidant.[5–7] It is known that these observed activities are dependent on the substituents attached to both ring A and B, where an electron-withdrawing group especially emphasizes the anti-cancer activity. The unique molecular structures and low toxic biological activities of chalcones have attracted a great deal of attention in organic chemistry, and there are many reports on the synthesis of their derivatives for pharmaceutical and food applications.[8–19]

With this background, however, little attention has been paid to water-soluble chalcones, which have the potential to exhibit novel biological activities. In this study, we focused on a chalcone diol, in which its two OH groups are directly attached to the phenyl ring A and B, with the expectation that an anionic charge generated due to deprotonation delocalizes over its π-conjugated structure. We have synthesized a series of chalcone derivatives by modifying the substituent on ring A and B, and found that the chalcone diol derivatives bearing OH group at the 2-position on both phenyl rings show visible color changes upon ionization in a polar solvent. The chalcone diol is colorless in water and becomes yellow at pH ≥ 10, whereas it is red in CH_3CN upon the addition of fluoride ions. Chalcone diols can serve as pH and F^- sensing dyes. Since the fluoride ion plays important roles in human health, F^- sensing especially has attracted much attention in biological, medicinal, environmental research fields.[20,21] Actually, a variety of the F^- sensing dyes including amide, indole, pyrrole, urea groups have been reported.[22–25] However, there are a few examples with the natural

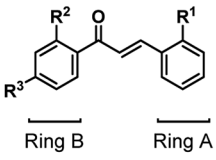

CLN	R^1	R^2	R^3
1	OH	OH	OCH_3
2	H	H	OCH_3
3	H	OH	OCH_3
4	OH	H	OCH_3
5	OH	OH	H
6	OH	OH	F

Chart 1 Chalcone derivatives CLN**1**–**6**.

[a]*Department of Pharmaceutical Sciences, Inner Mongolia Medical University, Jinshan Economic & Technology Development District, Hohhot, Inner Mongolia, 010110, China. E-mail: 20030091@immu.edu.cn*

[b]*Department of Chemistry, Graduate School of Science, Kobe University, 1-1 Rokkodai-cho, Nada-ku, Kobe 657-8501, Japan. E-mail: tsuda@harbor.kobe-u.ac.jp*

† Electronic supplementary information (ESI) available: UV-vis absorption spectra, ^1H and ^{13}C NMR spectroscopic data, HRMS. CCDC 1561801. For ESI and crystallographic data in CIF or other electronic format see DOI: 10.1039/d0ra06719a

biological compound such as chalcone. We herein revealed that the observed chemical coloration of the chalcone diols originates from their characteristic resonant π-conjugated structures generated upon the interaction of their OH groups and anions.

Results and discussion

We have synthesized a series of chalcones CLN**1–6** bearing hydrophilic OH, electron-donating OCH_3 and electron-withdrawing F substituents (Chart 1). These chalcone derivatives were synthesized *via* a base-catalyzed condensation of acetophenone and benzaldehyde bearing substituent groups in an ethanol solution by reference to the literature methods.[1] The products were characterized by means of ^1H and ^{13}C NMR and mass spectroscopy (see ESI†).

Molecular structure of CLN1

We obtained a single crystal of a CLN**1** through crystallization from ethanol, and then performed X-ray crystallographic analysis (Fig. 1). In the crystal structure, C–C bond lengths of C5–C6, C6–C7, C7–C8, and C8–C9 were 1.46, 1.45, 1.33, and 1.45 Å, respectively, and the C–O bond lengths for C2–O1, C4–O2, C6–O3, and C10–O4 were 1.36, 1.35, 1.26, and 1.36 Å respectively. These bond lengths are reasonable in that phenyl ring A and B are bridged by an α,β unsaturated carbonyl group. CLN**1** also adopts a planar conformation with dihedral angles of 3.3°, 3.9°, 0.4°, 4.1° and 6.3° for C4–C5–C6–C7, C5–C6–C7–C8, C6–C7–C8–C9, O3–C6–C7–C8, and C7–C8–C9–C10 respectively. The π-orbital and intramolecular hydrogen bonding interactions between the OH and the carbonyl groups may allow this planar conformation. The signal of OH proton at ring B in ^1H NMR spectrum of CLN**1** actually appeared at low magnetic field region $\delta = 13.56$ ppm, indicating the intramolecular hydrogen bonding interaction.

Halochromism of chalcone derivatives

We initially studied the optical and electronic properties of a chalcone diol CLN**1**, bearing an OCH_3 group on ring B and one OH group on both ring A and B, in water. The solid sample of CLN**1** is hardly soluble in water, but soluble in polar organic solvents, such as alcohols and acetonitrile. Then, we prepared its sample solution with a concentration of 4.0×10^{-5} mol L^{-1} upon fifty times dilution of a CH_3CN solution of CLN**1** in volume with water. The sample solution was colorless at pH = 1–6, but slightly colored at pH = 7–9. However, it became vivid yellow at pH ≥ 10 (Fig. 2a). The decolorization and coloration reversibly occurred upon addition of HCl and NaOH to the sample solution, respectively. Fig. 2b shows the corresponding absorption spectra of CLN**1** at pH = 1, 7, and 14. The spectra recorded for the sample solutions of CLN**1** at pH = 1 and 7 were almost identical with three absorption bands observed at λ_{max} = 278, 317, and 366 nm. Interestingly, the lowest energy absorption band was highly red-shifted to the visible region with λ_{max} = 434 nm at pH ≥ 10. This halochromic behavior may originate

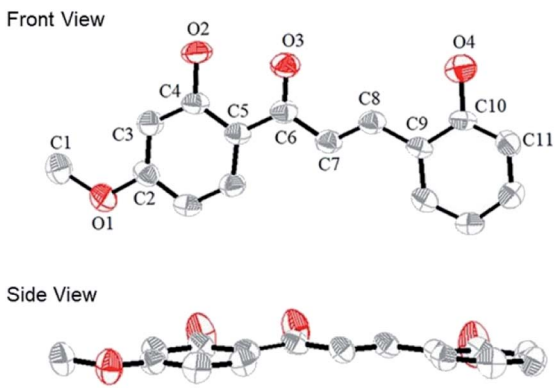

Fig. 1 The ORTEP diagram of CLN**1**, with ellipsoids set at 50% probability. The hydrogen atoms are omitted for clarity. The gray and red atoms represent the C and O atoms, respectively.

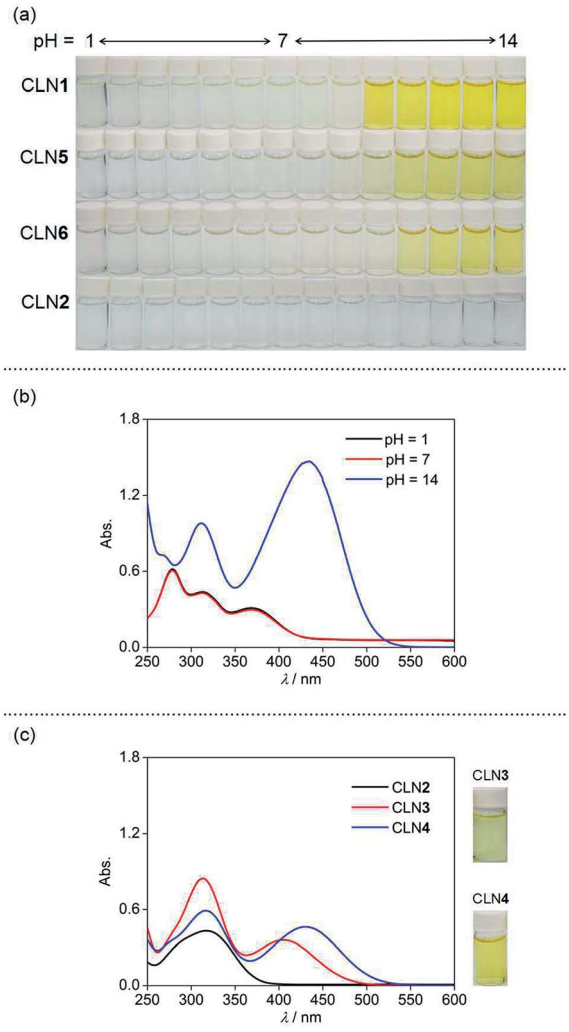

Fig. 2 (a) The pH dependent color changes of CLN**1**, **2**, **5**, and **6** in water (pH = 1–14). (b) The UV-vis absorption spectra of CLN**1** at 298 K in water with pH = 1, 7 and 14. (c) The UV-vis absorption spectra of CLN**2**, **3**, and **4** at 298 K in water with pH = 14. The sample solutions were prepared upon fifty times dilution of a CH_3CN solution of CLN**1–6** in volume with water. [CLN] = 4.0×10^{-5} mol L^{-1}.

from the ionization of CLN**1** due to the deprotonation of OH group on ring A and/or B under alkaline conditions (Scheme 1).

This proposed mechanism is supported by the fact that a reference compound CLN**2** without any OH groups showed no color change (Fig. 2a) and no red-shift in the absorption band even at pH = 14 (Fig. 2c). In contrast, chalcones CLN**3** and CLN**4**, bearing a single OH group on ring B and A, respectively, were both colored under alkaline conditions (Fig. 2c). The former compound showed a relatively smaller red-shifted the lowest energy absorption band with λ_{max} at 405 nm than that of latter one with λ_{max} at 430 nm at pH = 14 (Fig. 2c). The deprotonation of the OH group on ring A, which allows long range resonant π-electronic interactions to occur, may bring about a larger red-shift of the absorption band rather than that occurs on ring B (Scheme 1). With this reason, the color of CLN**3** observed may be lighter than that of CLN**1** and CLN**4**. The higher absorbance of the lowest energy band of CLN**1** may originate from the substituent effects of the OH group on ring B and its planar conformation due to the intramolecular hydrogen bonding interactions described above.

The colored pH region was also dependent on the substituent. For example, chalcones CLN**5** and CLN**6** without a substituent group and with an electron withdrawing F group on ring B, respectively, showed shifts of the colored region to higher pH. This can be explained by the competitive deprotonation of the phenolic OH groups on ring A and B. Since the acidity of the phenolic OH generally decreases in the presence of an electron donating OCH_3 group, and *vice versa* with an electron withdrawing F group, a relatively low contribution of ring B is expected for CLN**1** in the competitive deprotonation. However, CLN**6** contrary allows withdrawing of the anionic charge to ring B to increase its contribution, resulting in the shift of the colored region to pH ≥ 10.

Visible coloration of CLN upon F^- sensing in acetonitrile

The visible color change of CLN with anionic salts such as NaF has never been observed in water. We then investigated the chromic behaviors of the series of chalcone derivatives in an organic solvent upon the addition of 5 equiv. amounts of anionic salts. Representatively, CLN**1** bearing two OH groups showed a selective vivid red-coloration upon the addition of tetrabutylammonium fluoride (TBAF) in CH_3CN (Fig. 3a). However, no notable coloration of CLN**1** was observed with other TBA salts of Cl^-, Br^-, I^-, NO_3^-, and HSO_4^-, and slight coloration was observed with AcO^- and $H_2PO_4^-$. Furthermore, it also showed no color change upon mixing with NaF and KF, having strong ionic bonds compared with that of TBAF. The observed coloration of a mixture of CLN**1** and TBAF disappeared upon the addition of water or metal cations such as Al^{3+}, Zn^{2+}, Ba^{2+}, Fe^{2+} and Pb^{2+} to the sample solution, indicating that CLN**1** interacts directly with F^- without the formation of HF (g) and a possible salt of $TBA^+ \cdot CLN\mathbf{1}^-$. CLN**2** bearing no OH substituents showed no coloration in the presence of TBAF (Fig. 3b). However, CLN**3** and CLN**4** bearing one OH substituent on ring B and A, respectively, showed a light yellow and vivid orange color upon the addition of TBAF, respectively (Fig. 3c and d, respectively). These results suggest that the electrostatic interaction between the OH group and F^- especially in ring A, triggers the visible coloration of these chalcone derivatives. CLN**5** and CLN**6**, both have two OH groups, without and with an electron withdrawing halogen group respectively, also showed similar colorations as observed in the case of CLN**1** (Fig. 3e and f). Although the chalcone diols also showed such colorations in lower polarity solvents such as CH_2Cl_2, low solubilities of the inorganic salts did not allow further experiments for investigation.

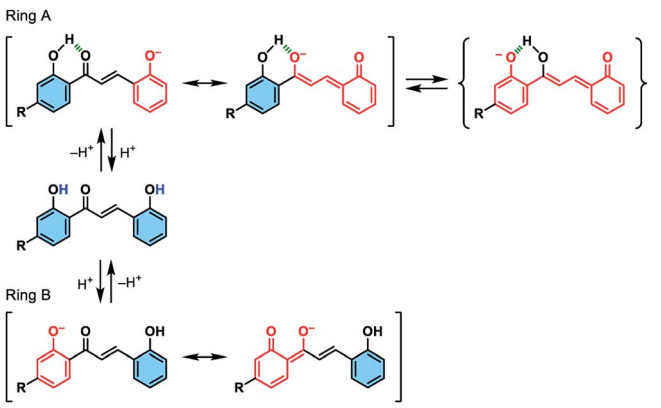

Scheme 1 Schematic illustrations of the possible ionizations of chalcone diols at ring A and B, and their resonant π-electronic structures.

Absorption spectral study

The corresponding UV-vis absorption spectral changes of CLN**1**, **3**, and **4** upon titration with TBAF are shown in Fig. 4. The

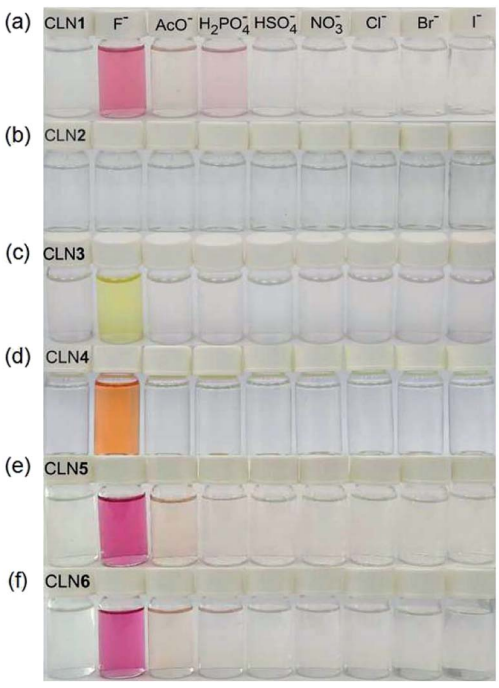

Fig. 3 The selective colorations of CLN**1–6** (4.0×10^{-5} mol L^{-1}), corresponding to (a)–(f) respectively, in CH_3CN at 298 K upon the addition of 5 equiv. amounts of TBA salts ($[Bu_4N^+]A^-$, $A^- = NO_3^-$, HSO_4^-, $H_2PO_4^-$, AcO^-, F^-, Cl^-, Br^-, I^-).

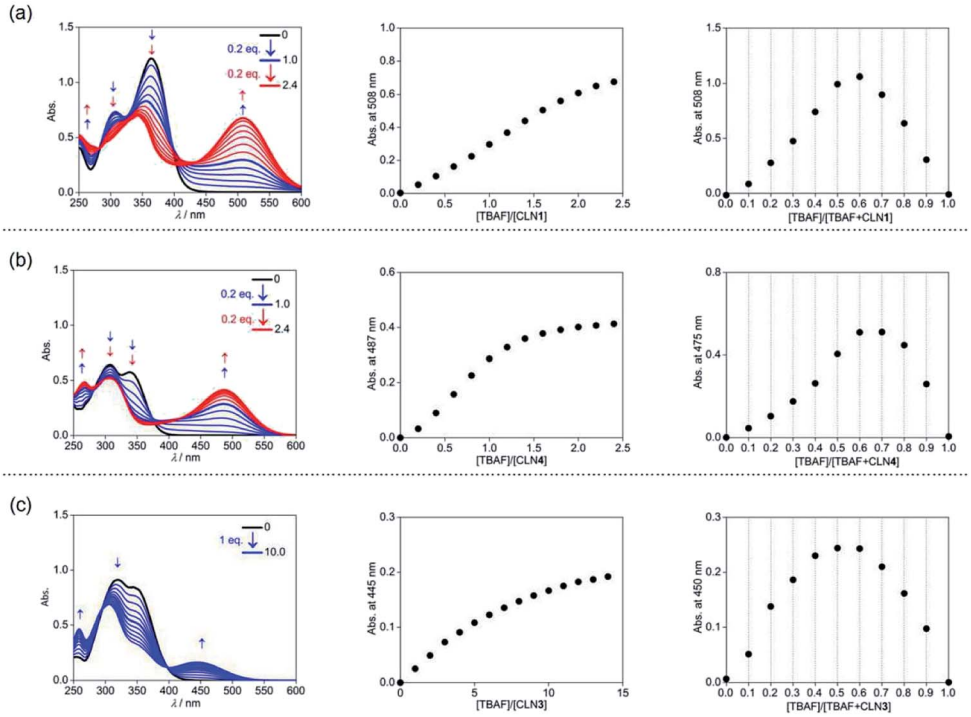

Fig. 4 UV-vis absorption spectral titrations of (a) CLN**1**, (b) CLN**4**, and (c) CLN**3** (4.0×10^{-5} mol L^{-1}) with TBAF in CH_3CN at 298 K (left), plots of the absorbance change at λ_{max} with respect to [TBAF]/[CLN] (center), and Job plots for the absorbance changes with respect to [TBAF]/[TBAF + CLN] (right).

lowest energy absorption band of CLN**1** with $\lambda_{max} = 363$ nm was dramatically red-shifted to 508 nm with expense of its original absorption bands upon titration with TBAF, and the profile shows a stepwise red-shifts of isosbestic points at 400 (0–1.0 equiv.), and 448 nm (1.0–2.4 equiv.) (Fig. 4a). The plot of the absorbance of λ_{max} with respect to the equivalent of added TBAF shows almost linear profile, and then, curved one before and after [TBAF]/[CLN**1**] = 1.0. The Job plot shows a maximum change at [TBAF]/[CLN**1** + TBAF] = 0.6. These results suggest that CLN**1** most likely allows a stepwise binding with two fluoride ions in the solution. The first 1 : 1 binding is very strong with $K_1 > 10^6$ M^{-1}, and the second 1 : 2 binding was calculated to be $K_2 = 2.1 \times 10^3$ M^{-1} (Table 1).

The titration experiments with TBAF were then conducted for CLN**4**, bearing a OH group on ring A (Fig. 4b). It exhibits the lowest energy absorption band at 351 nm, which was relatively higher energy with smaller absorbance compared with that of CLN**1**. Its absorption spectra upon titration with TBAF also showed a large red-shifted the lowest energy absorption band at $\lambda_{max} = 475$ nm, which was relatively higher energy than that observed in CLN**1** (Fig. 4b). In this profile, multi isosbestic points were not identified, but interestingly, a sigmoidal curve that indicates an allosteric effect in the binding was observed in the plot of the absorbance change with respect to [TBAF]/[CLN**4**]. The Job plot also shows a maximum absorbance change at around 0.6–0.7, indicating that CLN**4** binds two fluoride ions even though it only has one OH group in its structure. The binding constant $K_2 = 1.5 \times 10^6$ M^{-1} was actually obtained from the curve-fitting calculation.

Table 1 Binding constants K_1 and K_2 for the 1 : 1 and 1 : 2 interactions of CLN**1**–**6** and TBAF in CH_3CN at 298 K

	Binding constants (M^{-1})	
CLN	K_1	K_2
1	$>10^6$	2.1×10^3
2	—[a]	—[a]
3	2.5×10^4	—[a]
4	—[b]	1.5×10^6
5	$>10^6$	8.0×10^3
6	$>10^6$	1.1×10^4

[a] No binding. [b] Allosteric binding.

The titration of CLN**3** with TBAF, having a spectral pattern similar to that of CLN**4**, also showed the red-shift of the lowest energy absorption band to $\lambda_{max} = 450$ nm with expense of its original absorption bands at $\lambda_{max} = 352$ nm (Fig. 4c). However, the observed red-shift and absorbance of the band are clearly smaller than those observed in CLN**1** and CLN**4**. Furthermore, the titration profile shows clear isosbestic points at 296 and 398 nm, which show no shifts until the saturation (~10 equiv. of TBAF). The Job plot provides a maximum absorbance change at 0.5, indicating a 1 : 1 binding interaction. The binding constant of CLN**3** and TBAF was calculated to be $K_1 = 2.5 \times 10^4$ M^{-1}, which is smaller than that of CLN**1** and K_2 of CLN**4**. CLN**5** and CLN**6** showed relatively larger red-shifts to 515 and 517 nm, respectively, upon titration with TBAF, and the resulting titration profiles also provided two-step shifts of the isosbestic points (Fig. S1†), as observed in the case of

CLN**1**. In addition, their Job plots also indicated a 1 : 2 binding interaction (Fig. S1†). Then, their binding constants with TBAF were calculated to be $K_2 = 8.0 \times 10^3$ M^{-1} for CLN**5** and $K_2 = 1.1 \times 10^4$ M^{-1} for CLN**6**, which are larger than that of CLN**1**. The electron withdrawing substituent may enhance the acidity of the OH groups to accelerate interactions of CLN with F^-, but *vice versa* with an electron donating group. However, CLN**1**, **5** and **6** do not show the allosteric effect in the complexation, it is most likely due to their strong 1 : 1 binding interaction with F^-, which may electrically reduce the second binding of F^- to give a larger K_1 than K_2.

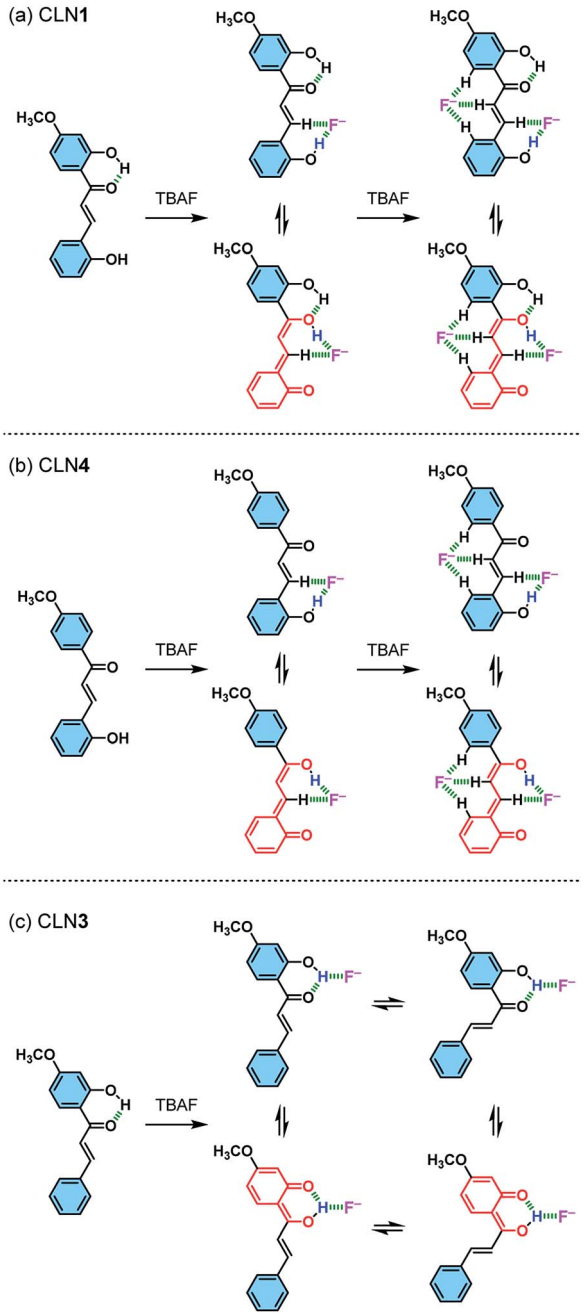

Scheme 2 Schematic illustrations of the possible interactions formed between (a) CLN**1**, (b) CLN**4**, and (c) CLN**3** and F^-, and their resonant π-electronic structures.

The red-shifted absorption bands of the chalcone derivatives appear in the visible region upon the addition of TBAF are most likely originated from their π-electronic resonant structures formed *via* the interaction of OH group with F^- (Scheme 2). The magnitude of the red-shifts observed in the order of CLN**1** > CLN**4** > CLN**3** are reasonably explained by the attached substituent group, resonant π-electronic conjugations between OH groups and carbonyl group, and the conformation of the components that allows π-orbital interactions. CLN**1**, CLN**4**, and CLN**3** increase anionic characters through interaction of OH and F^-. The CLN**4** anion allows long range resonance over the phenol ring A and the α,β-unsaturated carbonyl group, resulting in a larger red-shift of the absorption band than CLN**3**, which includes a carbonyl group that directly attaches to the phenol ring B. While CLN**1**, bearing two phenol rings, may allow extension of the π-electronic structure and enhancement of the planarity due to intramolecular hydrogen bonding to result the larger red-shift of the absorption band than CLN**4**. However, the similar absorption spectral pattern of CLN**1**·2F^- complex with that of CLN**4**·2F^- complex (Fig. 4a and b) indicates that both CLN**1** and CLN**4** form similar 1 : 2 complexes with TBAF.

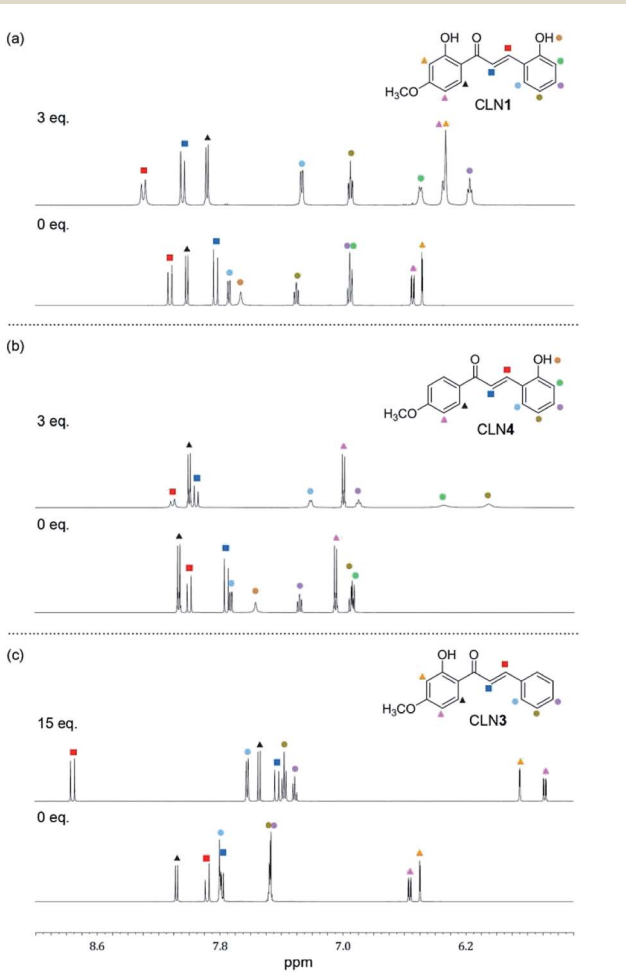

Fig. 5 The changes observed in the ^{1}H NMR spectra (600 MHz) of (a) CLN**1**, (b) CLN**4**, and (c) CLN**3** (1.4×10^{-2} mol L^{-1}) upon titration with TBAF in CD_3CN at 293 K.

^{1}H NMR spectral study

CLN**4** may bind to F^- due to the acidic hydrogen atoms in the OH and β-CH group, which accelerate proton transfer (PT) from the phenolic OH to the carbonyl group (Scheme 2b). PT accompanies resonant π-conjugation to give the dramatic spectral changes. This complexation locks potential rotation of the ring A, which may allow the entropically favorable additional binding of F^- to form a 1 : 2 complex. As a support of this proposed mechanism, the ^{1}H NMR spectrum of CLN**4** in CD_3CN actually shows characteristic peak shifts of the complexation upon the addition of 3 equiv. amounts of TBAF (Fig. 5b). The signal of OH group on ring A is disappeared, it is most likely due to the interaction with F^-, and the other signals of the phenol ring were shifted to the high magnetic field region which were clearly larger than those of ring B. On the contrary, the signals of the α- and β-protons on alkenyl group were shifted to the low magnetic field, which may originate from the resulting resonant π-conjugation and deshielding effects of ring A and B. These spectral changes indicate that CLN**4** adopts a rigid planar conformation in the 1 : 2 complexation, where the second F^- may stabilize the structure of the complex *via* multiple CH–F^- interactions in the formed cavity (Scheme 2b, right). The locked conformation of the 1 : 1 complex may play a crucial role during the formation of its subsequent 1 : 2 complex, because CLN**2** shows no peak shifts in its ^{1}H NMR spectrum upon the addition of an excess amount of TBAF (Fig. S2†).

On the other hand, binding CLN**3** with TBAF exhibits a smaller binding constant K_1 (Fig. 4c), which is explained by the weaker interaction of F^- and the phenolic OH, having lower acidity due to intramolecular hydrogen bonding with the adjacent carbonyl group (Scheme 2). The smaller local resonant π-conjugation structure of CLN**3**·F^-, which provides lower stability, may also reduce the binding constant K_1. Furthermore, the 1 : 1 complex CLN**3**·F^- hardly forms a 1 : 2 complex, since it may allow the rotation of the two C–C bonds attached on the α,β-unsaturated alkenyl group. The ^{1}H NMR spectrum of CLN**3** upon the addition of 15 equiv. amounts of TBAF also supports the proposed mechanism (Fig. 5c). The signal of the OH group on ring B at 13.43 ppm is disappeared, it is most likely due to the interaction. The other signals of ring B were also shifted to the high magnetic field region which are clearly larger than those of ring A. The signal of the α-proton on the alkenyl group was shifted to the high magnetic fields, however, the β-proton signal shows a low magnetic field shift. These characteristic shifts may be also responsible for the resulting resonant structure formed *via* PT (Scheme 2c). This breaks the π-conjugation of the α,β-unsaturated carbonyl group, resulting in unlocking of the C–C bond rotation between carbonyl and α-carbons. The β-proton undergoes deshielding effects from ring A, resulting in the peak shift to low magnetic field region.

Judging from the strong affinity with F^- of CLN**4** than that of CLN**3**, it was expected that CLN**1**, although having two OH groups, binds to F^- dominantly at ring A when forming the initial 1 : 1 complex (Scheme 2a). Furthermore, the extremely large K_2 of CLN**4** also supports our expectation that CLN**1** forms a similar 1 : 2 complex with TBAF. The ^{1}H NMR spectrum of CLN**1** upon the addition of 3 equiv. amounts of TBAF (Fig. 5a) actually shows similar spectral changes as observed in CLN**4**. The signals corresponding to the phenol ring A show higher magnetic field shifts than that of ring B. In addition, the signals of the α- and β-protons on the alkenyl group are shifted to the low magnetic field. The 1 : 1 complex of CLN**1** and F^- may bind an additional F^- by multiple CH–F^- interactions in the formed cavity rather than OH–F^- interaction on ring B.

DFT calculations

The lowest energy absorption band of CLN**1** appeared at λ_{max} = 363 nm in CH_3CN was slightly blue-shifted to 361 nm in CH_2Cl_2 (Fig. S3†). However, the absorption band at λ_{max} upon the addition of TBAF was further red-shifted to 508 and 513 nm in CH_3CN and CH_2Cl_2, respectively. This result can be attributed to an intramolecular charge transfer (CT) absorption band.[26,27] The CT may occur from the electron donating OH–F^- group to the electron accepting carbonyl group *via* the π-conjugated structure. This hypothesis was supported by density functional theory (DFT) and time-dependent DFT (TD-DFT) calculations at the B3LYP/6-311++g(d,p) level with the Gaussian 16 program package Revision A.03 (Fig. 6).[28] The calculated absorption spectrum obtained for CLN**1** using TD-DFT shows two bands (λ_{max} = 300 and 368 nm) and is essentially identical the experimental spectrum (λ_{max} = 308 and 363 nm) (Fig. 6a). Frontier Molecular Orbitals (FMO) calculations also reveal that the highest occupied molecular orbital (HOMO) and the lowest unoccupied molecular orbital (LUMO) of CLN**1** mainly consist

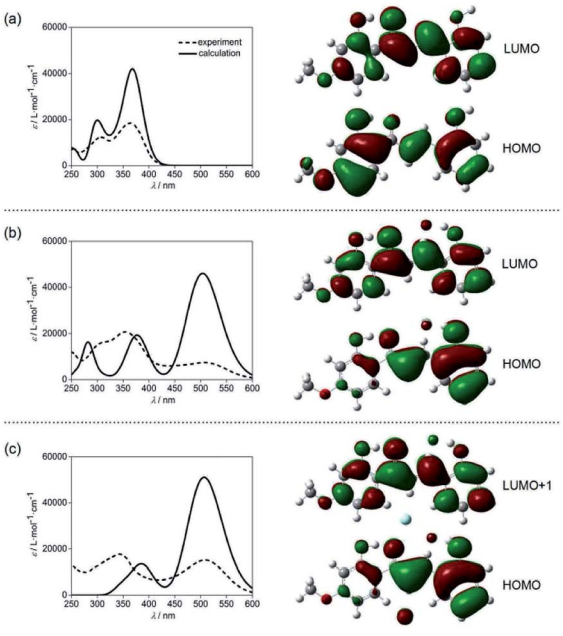

Fig. 6 DFT calculations of the electronic absorption spectra and HOMO and LUMO of (a) CLN**1**, (b) CLN**1**·F^-, and (c) CLN**1**·2F^- at the B3LYP/6-311++g(d,p) level. The calculations were demonstrated with X-ray crystallographic data of CLN**1** with OH–F^- distance = 1.34 Å.

Table 2 Crystallographic data obtained for CLN1

Chemical formula	$C_{16}H_{14}O_4$
Formula weight	267.27
Crystal system	Monoclinic
Space group	$P2_1/c$
Temperature (K)	293.15
Wavelength (Å)	1.54178
a (Å)	13.1097(7)
b (Å)	8.0041(5)
c (Å)	14.2334(8)
α (°)	90
β (°)	117.105(3)
γ (°)	90
Calculated density (g cm^{-3})	1.335
Volume (Å^3)	1329.50(14)
Z	4
Independent reflections	1528
Absorption coefficient (mm^{-1})	0.762
F(000)	560.0
2θ range (°)	7.58 to 105.42
Index ranges	$-13 \le h \le 13$, $-8 \le k \le 7$, $-14 \le l \le 14$
Goodness-of-fit on F^2	1.061
Final R indexes [$I > 2\sigma$ (I)]	$R_1 = 0.0605$, w$R_2 = 0.1583$
Final R indices (all data)	$R_1 = 0.0790$, w$R_2 = 0.1716$
Largest diff. peak/hole/e Å^{-3}	0.90/−0.22

of the π- and π*-systems over the chalcone backbone including its substituents. The lowest energy absorption originates from the electronic transition from HOMO to LUMO with a 96% contribution.

On the other hand, the calculations of CLN**1**·F$^-$, which includes an OH–F$^-$ interaction on ring A, provided the largest energy band at 503 nm, and two smaller bands at 374 and 282 nm (Fig. 6b). This spectral pattern and the wavelengths of the peak maxima also coincide with its experimental spectrum (286, 356, and 508 nm). The calculations also reveal that the lowest energy band can be attributed to the HOMO–LUMO transition with a 97% contribution. MOs calculations showed that phenol ring A together with the bound F$^-$ contribute to the HOMO of CLN**1**·F$^-$, whereas, ring B has little contribution. These results suggest that the strong red-shifted absorption band of CLN**1**·F$^-$ that appears in the visible region originates from the CT.

With these basic calculations of CLN**1**·F$^-$, we then demonstrated the calculations of CLN**1**·2F$^-$, which probably includes a second F$^-$ in the formed cavity *via* multiple CH–F$^-$ interactions. The calculated spectrum shows two bands at 505 and 389 nm (Fig. 6c). Compared with CLN**1**·F$^-$, the lowest energy band was slightly blue-shifted with increased intensity, while the other higher energy bands were unified with decreased intensity. The lowest energy band originates from the HOMO to LUMO+1 with an 82% contribution. The features observed in the calculated spectra are also essentially identical to its experimental spectrum (343 and 508 nm). The results strongly support our proposed mechanism for the 1 : 2 complexation of CLN**1** with TBAF.

Conclusions

Herein, we have reported a novel function of hydroxychalcone dyes that serve as a color indicator for pH and fluoride ions. The chalcone diol CLN**1**, bearing OH groups at the 2-positions on ring A and B, respectively, shows a vivid color change from colorless to yellow (halochromism) in water at pH ≥ 10. The colored region is shifted to higher pH, when using CLN**5** and **6**, having no substituent group and an electron-withdrawing F group, respectively, at the 4-position on ring B. Furthermore, these chalcone diols showed selective vivid colorations from colorless to red upon the addition of TBAF in an organic solvent, such as CH_3CN. CLN**1** provides a strong red-shifted absorption band in the visible region in alkaline aqueous solution and upon the addition of TBAF in CH_3CN. The characteristic large π-resonant structures of the chalcone were enhanced *via* ionization and the OH–F$^-$ interaction, respectively, which may allow light absorption due to charge transfer (CT) transition. This proposed mechanism has also been supported using TD-DFT calculations for CLN**1**, which represents observed absorption spectral features of characteristic frontier molecular orbitals upon its 1 : 1 and 1 : 2 interactions with F$^-$. X-ray crystallographic study and spectroscopic titration experiments in absorption and ^{1}H NMR spectra recorded for CLN, in comparison with reference CLN**2**, CLN**3**, and CLN**4**, revealed that the selective vivid colorations of the chalcone diols observed for F$^-$ may originate from the following three factors: (1) the strong OH–F$^-$ interaction on ring A, (2) 1 : 2 complexation of the chalcone diol and TBAF and (3) the planar structure of the chalcone diol owing to the π-conjugation structure and hydrogen-bonding between the phenolic OH group on ring B and the carbonyl group.

The observed results and mechanisms for the coloration of the hydroxychalcone derivatives, caused by ionization and selective anion recognition, may provide future strategies for the molecular design of chalcone-based chemical sensors and bioactive chemical substances.

Experimental section

General experimental materials

Unless stated otherwise, all reagents and solvents were used as received from Tokyo Chemical Industry Co., Ltd. (TCI) [ethanol (>99%), methylene chloride (>99%), 2-hydroxyl-4-methoxyl-acetophenone (>99%), 3-hydroxyl-4-methoxyl-acetophenone (>99%), phenylaldehyde (>99%), 2-hydroxyl-4-methoxyl-acetophenone (>99%), acetonitrile-D (>99%), 2-hydroxyacetophenone (>99%), potassium hydroxide (>99%), 4-fluoro-2-hydroxyacetophenone (>99%), 2-hydroxybenzaldehyde (>99%), and TBA salts (([Bu_4N^+]A$^-$, A$^-$ = NO_3^-, HSO_4^-, $H_2PO_4^-$, AcO$^-$, F$^-$, Cl$^-$, Br$^-$, I$^-$) (>99%))], TianJin YongDa Chemical Reagent Company Limited [NaF (>99%)], Adamas Reagent Co., Ltd. [KF (>99%)], Acros Organics [Pb(ClO_4)$_2$ (>99%)], Shanghai Macklin Biochemical Co., Ltd. [Ba(ClO_4)$_2$ (>99%), Al(ClO_4)$_3$ (>99%)], Shanghai Aladin Biochemical Technology Co., Ltd. [Zn(ClO_4)$_2$ (>99%), Fe(ClO_4)$_2$ (>99%)].

Crystallographic data

The crystallographic data obtained for CLN**1** are reported in Table 2.

Measurements and calculations

^{1}H and ^{13}C NMR spectra were recorded on Bruker AVANCE 600 and 500 spectrometers, where chemical shifts (δ in ppm) were determined with respect to tetramethylsilane as an internal standard. The absorption spectra were recorded on a UV spectrometer equipped with a Shimadzu temperature/stirring controller. All calculations were carried out by the density functional theory (DFT) and time-dependent DFT (TD-DFT) calculations at the B3LYP/6-311++g(d,p) level with the Gaussian 16 program package Revision A.03.

Synthesis

CLN1. 4-Methoxyl-2-hydroxyl-acetophenone (1.66 g, 10 mmol) was dissolved in 2.5 mL of 95% ethanol, and 5 mL of 50% potassium hydroxide aqueous solution was then added to the sample solution. The mixture was stirred for 10 min at 30 °C until all the solutes were dissolved to give a homogeneous solution. After then, 2-hydroxybenzaldehyde (1.22 g, 10 mmol) was dissolved in 2.5 mL of 95% ethanol and slowly added to the mixture. The resulting solution was then refluxed for 36 h. After completion of the reaction, the pH was adjusted to 2 with dilute hydrochloric acid and extracted with CH_2Cl_2. The combined organic layers were dried over anhydrous Na_2SO_4 and evaporated to dryness. CLN**1** was isolated as a yellow solid through silica gel column chromatography with CH_2Cl_2 and methanol (50 : 1, v/v) as an eluent in 35% yield (0.95 g, 3.5 mmol). ^{1}H NMR (600 MHz, CD_3CN, 293 K) δ (ppm): 13.54 (s, 1H), 8.13 (d, J = 15.6 Hz, 1H), 8.02 (d, J = 9.0, 1H), 7.83 (d, J = 15.6 Hz, 1H), 7.74 (dd, J = 7.8, 1.7 Hz, 1H), 7.66 (s, 1H), 7.30 (td, J = 7.8, 1.6 Hz, 1H), 6.96 (t, J = 7.8 Hz, 1H), 6.95 (d, J = 7.8 Hz, 1H), 6.55 (dd, J = 9.0, 2.6 Hz, 1H), 6.48 (d, J = 2.6 Hz, 1H), 3.86 (s, 3H); ^{13}C NMR (150 MHz, CD_3CN, 293 K) δ (ppm): 193.18, 167.02, 166.80, 157.17, 139.94, 132.67, 132.59, 129.86, 121.04, 120.94, 116.72, 114.54, 107.78, 101.51, 56.08. HRMS (Orbitrap) m/z: $[M - H]^-$ calculated for $C_{16}H_{14}O_4$: 269.0808, found: 269.0807.

CLN2. 4-Methoxyl-acetophenone (1.50 g, 10 mmol) was dissolved in 2 mL of 95% ethanol. After then, benzaldehyde (1 mL, 10 mmol) was dissolved in 2 mL of 95% ethanol and slowly added to the sample solution. The mixture was then refluxed for 12 h. After completion of the reaction, the pH was adjusted to 2 with dilute hydrochloric acid and extracted with ether. The crude product was washed with ethanol to give CLN**2** as a white solid in 49% yield (1.17 g, 5 mmol). ^{1}H NMR (500 MHz, CD_3CN, 293 K) δ (ppm): 8.09 (d, J = 9.0 Hz, 2H), 7.76 (dd, J = 7.5, 1.4 Hz, 1H), 7.75 (d, J = 14.4 Hz, 1H), 7.71 (d, J = 15.5 Hz, 1H), 7.48–7.43 (m, 3H), 7.05 (d, J = 8.0 Hz, 2H), 3.88 (s, 3H); ^{13}C NMR (125 MHz, CD_3CN, 293 K) δ (ppm): 187.99, 163.62, 143.05, 135.19, 130.95, 130.78, 130.34, 128.96, 128.48, 122.18, 113.91, 55.35. HRMS (Orbitrap) m/z: $[M + Na]^+$ calculated for $C_{16}H_{14}O_2$: 261.0886, found: 261.0888.

CLN3. 4-Methoxyl-2-hydroxyl-acetophenone (1.43 g, 8.6 mmol) was dissolved in 2 mL of 95% ethanol, and 5 mL of 50% potassium hydroxide aqueous solution was then added to the sample solution. The mixture was stirred for 10 min at 30 °C until all the solutes were dissolved to give a homogeneous solution. After then, benzaldehyde (1 mL, 8.5 mmol) was dissolved in 2 mL of 95% ethanol and slowly added to the mixture. The resulting solution was then refluxed for 36 h. After completion of the reaction, the pH was adjusted to 5–6 with dilute hydrochloric acid and extracted with CH_2Cl_2. The combined organic layers were dried over anhydrous Na_2SO_4 and evaporated to dryness. CLN**3** was isolated as a yellow solid through silica gel column chromatography with CH_2Cl_2 as an eluent in 20% yield (0.43 g, 1.7 mmol). ^{1}H NMR (500 MHz, CD_3CN, 293 K) δ (ppm): 13.41 (s, 1H), 8.07 (d, J = 9.0 Hz, 1H), 7.87 (d, J = 15.5 Hz, 1H), 7.85 (dd, J = 6.5, 2.7 Hz, 2H), 7.77 (d, J = 15.7 Hz, 1H), 7.48–7.45 (m, 3H), 6.60 (dd, J = 9.1, 2.3 Hz, 1H), 6.49 (dd, J = 9.1, 2.3 Hz, 1H), 3.86 (s, 3H); ^{13}C NMR (125 MHz, CD_3CN, 293 K) δ (ppm): 192.31, 166.53, 144.00, 134.88, 132.24, 130.73, 129.00, 128.77, 120.89, 113.95, 112.70, 107.29, 101.01, 55.56. HRMS (Orbitrap) m/z: $[M - H]^-$ calculated for $C_{16}H_{14}O_3$: 253.0859, found: 253.0859.

CLN4. 4-Methoxyl-acetophenone (0.80 g, 5 mmol) was dissolved in 2 mL of 95% ethanol solution, and 2 mL of 20% potassium hydroxide aqueous solution was then added to the sample solution. The mixture was stirred for 10 min at 30 °C until all the solutes were dissolved to give a homogeneous solution. After then, 2-hydroxybenzaldehyde (0.61 g, 5 mmol) was dissolved in 2 mL of 95% ethanol and slowly added to the mixture. The resulting solution was then refluxed for 36 h. After completion of the reaction, the pH was adjusted to 2 with dilute hydrochloric acid and extracted with CH_2Cl_2. The combined organic layers were dried over anhydrous Na_2SO_4 and evaporated to dryness. CLN**4** was isolated as a green needle crystal through silica gel column chromatography with CH_2Cl_2 as an eluent in 24% yield (0.31 g, 1.2 mmol). ^{1}H NMR (500 MHz, CD_3CN, 293 K) δ (ppm): 8.06 (d, J = 8.9 Hz, 2H), 8.00 (d, J = 15.7 Hz, 1H), 7.75 (d, J = 15.5 Hz, 1H), 7.72 (dd, J = 8.0, 1.7 Hz, 1H), 7.67 (br, 1H), 7.28 (td, J = 7.7, 1.5 Hz, 1H), 7.04 (d, J = 9.0 Hz, 2H), 6.94 (t, J = 8.0 Hz, 1H), 6.93 (d, J = 7.8 Hz, 1H), 3.87 (s, 3H); ^{13}C NMR (125 MHz, CD_3CN, 293 K) δ (ppm): 188.45, 163.48, 156.38, 138.45, 131.64, 131.17, 130.67, 128.91, 122.10, 122.00, 120.40, 116.15, 113.87, 55.32. HRMS (Orbitrap) m/z: $[M - H]^-$ calculated for $C_{16}H_{14}O_3$: 253.0859, found: 253.0868.

CLN5. 2-Hydroxyacetophenone (1.36 g, 10 mmol) was dissolved in 2.5 mL of 95% ethanol solution, and 5 mL of 50% potassium hydroxide aqueous solution was then added to the sample solution. The mixture was stirred for 10 min at 30 °C until all the solutes were dissolved to give a homogeneous solution. After then, 2-hydroxybenzaldehyde (1.22 g, 10 mmol) was dissolved in 2.5 mL of 95% ethanol and slowly added to the mixture. The resulting solution was then refluxed for 30 h. After completion of the reaction, the pH was adjusted to 2 with dilute hydrochloric acid and extracted with CH_2Cl_2. The combined organic layers were dried over anhydrous Na_2SO_4 and evaporated to dryness. CLN**5** was isolated as a yellow solid through

silica gel column chromatography with CH_2Cl_2 as an eluent in 35% yield (0.84 g, 3.5 mmol). ^{1}H NMR (500 MHz, CD_3CN, 293 K) δ (ppm): 12.91 (s, 1H), 8.17 (d, J = 15.5 Hz, 1H), 8.09 (dd, J = 8.6, 1.6 Hz, 1H), 7.92 (d, J = 15.5 Hz, 1H), 7.75 (dd, J = 7.5, 1.6 Hz, 1H), 7.69 (s, 1H), 7.55 (td, J = 7.9, 1.6 Hz, 1H), 7.32 (td, J = 7.7, 1.6 Hz, 1H), 6.99 (td, J = 7.6, 1.5 Hz, 1H), 6.98 (t, J = 7.3 Hz, 1H), 6.97 (d, J = 7.3 Hz, 1H), 6.96 (d, J = 8.0 Hz, 1H); ^{13}C NMR (125 MHz, CD_3CN, 293 K) δ (ppm): 194.59, 163.37, 156.80, 140.53, 136.44, 132.39, 130.36, 129.53, 121.66, 120.45, 120.42, 120.04, 118.99, 117.99, 116.26. HRMS (Orbitrap) m/z: $[M - H]^-$ calculated for $C_{15}H_{12}O_3$: 239.0703, found: 239.0707.

CLN6. 4-Fluoro-2-hydroxyacetophenone (1.54 g, 10 mmol) was dissolved in 2.5 mL of 95% ethanol solution, and 5 mL of 40% potassium hydroxide aqueous solution was then added to the sample solution. The mixture was stirred for 10 min at 30 °C until all the solutes were dissolved to give a homogeneous solution. After then, 2-hydroxybenzaldehyde (1.22 g, 10 mmol) was dissolved in 2.5 mL of 95% ethanol and slowly added to the mixture. The resulting solution was then refluxed for 38 h. After completion of the reaction, the pH was adjusted to 2 with dilute hydrochloric acid and extracted with CH_2Cl_2. The combined organic layers were dried over anhydrous Na_2SO_4 and evaporated to dryness. CLN**6** was isolated as a yellow solid through silica gel column chromatography with CH_2Cl_2 as an eluent in 35% yield (0.90 g, 3.5 mmol). ^{1}H NMR (500 MHz, CD_3CN, 293 K) δ (ppm): 13.35 (s, 1H), 8.18 (d, J = 15.8 Hz, 1H), 8.16 (dd, J = 7.8, 5.6 Hz, 1H), 7.84 (d, J = 15.6 Hz, 1H), 7.74 (dd, J = 7.8, 1.5 Hz, 1H), 7.67 (br, 1H), 7.32 (td, J = 7.8, 1.5 Hz, 1H), 6.97 (td, J = 7.4, 2.1 Hz, 1H), 6.96 (d, J = 7.7 Hz, 1H), 6.76 (dd, J = 8.8, 2.5 Hz, 1H), 6.72 (dd, J = 10.6, 2.5 Hz); ^{13}C NMR (125 MHz, CD_3CN, 293 K) δ (ppm): 193.51, 156.85, 140.75, 133.17, 133.07, 132.49, 129.53, 121.58, 120.44, 120.24, 116.26, 106.96, 106.77, 104.46, 104.27. HRMS (Orbitrap) m/z: $[M - H]^-$ calculated for $C_{15}H_{11}O_3F$: 257.0608, found: 257.0615.

Conflicts of interest

The authors declare no conflict of interest.

Acknowledgements

The present work was sponsored by The National Natural Science Foundation of China (21961026).

Notes and references

1 B. Zhou and C. G. Xing, *Med. Chem.*, 2015, **5**, 388–404.
2 D. I. Batovska and I. T. Todorova, *Curr. Clin. Pharmacol.*, 2010, **5**, 1–29.
3 N. K. Sahu, S. S. Balbhadra, J. Choudhary and D. V. Kohli, *Curr. Med. Chem.*, 2012, **19**, 209–225.
4 C. Karthikeyan, N. S. Moorthy, S. Ramasamy, U. Vanam, E. Manivannan, D. Karunagaran and P. Trivedi, *Recent Pat. Anti-Cancer Drug Discov.*, 2015, **10**, 97–115.
5 C. L. Zhuang, W. Zhang, C. Q. Sheng, W. N. Zhang, C. G. Xing and Z. Y. Miao, *Chem. Rev.*, 2017, **117**, 7762–7810.
6 A. M. Katsori and D. Hadjipavlou-Litina, *Expert Opin. Ther. Pat.*, 2011, **21**, 1575–1596.
7 P. Singh, A. Anand and V. Kumar, *Eur. J. Med. Chem.*, 2014, **85**, 758–777.
8 G. Romanelli, G. Pasquale, A. Sathicq, H. Thomas, J. Autino and P. Vazquez, *J. Mol. Catal. Chem.*, 2011, **340**, 24–32.
9 M. J. Climent, A. Corma, S. Iborra and A. Velty, *J. Catal.*, 2004, **221**, 474–482.
10 J. Y. Park, J. A. Ko, D. W. Kim, Y. M. Kim, H. J. Kwon, H. J. Jeong, C. Y. Kim, K. H. Park, W. S. Lee and Y. B. Ryu, *J. Enzym. Inhib. Med. Chem.*, 2016, **31**, 23–30.
11 J. B. Daskiewicz, G. Comte, D. Barron, A. D. Pietro and F. Thomasson, *Tetrahedron Lett.*, 1999, **40**, 7095–7098.
12 V. R. Yadav, S. Prasad, B. Sung and B. B. Aggarwal, *Int. Immunopharmacol.*, 2011, **11**, 295–309.
13 K. V. Sashidhara, A. Kumar, M. Kumar, J. Sarkar and S. Sinha, *Bioorg. Med. Chem. Lett.*, 2010, **20**, 7205–7211.
14 L. B. Salum, W. F. Altei, L. D. Chiaradia, M. N. S. Cordeiro, R. R. Canevarolo, C. P. S. Melo, E. Winter, B. Mattei, H. N. Daghestani, M. C. Santos-Silva, T. B. Creczynski-Pasa, R. A. Yunes, J. A. Yunes, A. D. Andricopulo, B. W. Day, R. J. Nunes and A. Vogt, *J. Med. Chem.*, 2013, **63**, 501–510.
15 B. Kolundzija, V. Markovic, T. Stanojkovic, L. Joksovic, I. Matic, N. Todorovic, M. Nikolic and M. D. Joksovic, *Bioorg. Med. Chem. Lett.*, 2014, **24**, 65–71.
16 Y. L. N. Murthy, K. P. Suhasini, A. S. Pathania, S. Bhushan and Y. N. Sastry, *Eur. J. Med. Chem.*, 2013, **62**, 545–555.
17 I. Karpaviciene, I. Cikotiene and J. M. Padron, *Eur. J. Med. Chem.*, 2013, **70**, 568–578.
18 X. W. Zhou, H. L. Ma, X. Zhang, S. Y. Jing, J. Y. Miao and B. X. Zhao, *Eur. J. Med. Chem.*, 2014, **79**, 95–101.
19 V. Sharma, V. Kumar and P. Kumar, *Anti-Cancer Agents Med. Chem.*, 2013, **13**, 422–432.
20 M. G. Jaroslaw, S. Olga and J. Janusz, *Chem.–Eur. J.*, 2014, **20**, 12790–12795.
21 R. B. Sushil, M. Bijan, V. Gonela and T. Arunabha, *Inorg. Chem.*, 2017, **56**, 11577–11590.
22 S. O. Kang, J. M. Llinares, V. W. Day and K. Bowman-James, *Chem. Soc. Rev.*, 2010, **39**, 3980–4003.
23 J. L. Sessler, D. G. Cho and V. Lynch, *J. Am. Chem. Soc.*, 2006, **128**, 16518–16519.
24 V. Thiagarajan, P. Ramamurthy, D. Thirumalai and V. T. Ramakrishnan, *Org. Lett.*, 2005, **7**, 657–660.
25 Z. M. Yin, Y. H. Zhang, J. Q. He and J. P. Cheng, *Tetrahedron*, 2006, **62**, 765–770.
26 T. Viruthachalam, R. Perumal, T. Dhakshanamurthy and T. R. Vayalakkavoor, *Org. Lett.*, 2005, **7**, 657–660.
27 K. Imamura, Y. Ueno, S. Akimoto, K. Eda, Y. Du, C. Eerdun, M. Wang, K. Nishinaka and A. Tsuda, *ChemPhotoChem*, 2017, **1**, 427–431.
28 M. J. Frisch, G. W. Trucks, H. B. Schlegel, G. E. Scuseria, M. A. Robb, J. R. Cheeseman, G. Scalmani, V. Barone, G. A. Petersson, H. Nakatsuji, X. Li, M. Caricato, A. V. Marenich, J. Bloino, B. G. Janesko, R. Gomperts, B. Mennucci, H. P. Hratchian, J. V. Ortiz, A. F. Izmaylov, J. L. Sonnenberg, D. Williams-Young, F. Ding, F. Lipparini, F. Egidi, J. Goings, B. Peng, A. Petrone,T. Henderson,

D. Ranasinghe, V. G. Zakrzewski, J. Gao, N. Rega, G. Zheng, W. Liang, M. Hada, M. Ehara, K. Toyota, R. Fukuda, J. Hasegawa, M. Ishida, T. Nakajima, Y. Honda, O. Kitao, H. Nakai, T. Vreven, K. Throssell, J. A. Montgomery Jr., J. E. Peralta, F. Ogliaro, M. J. Bearpark, J. J. Heyd, E. N. Brothers, K. N. Kudin, V. N. Staroverov, T. A. Keith, R. Kobayashi, J. Normand, K. Raghavachari, A. P. Rendell, J. C. Burant, S. S. Iyengar, J. Tomasi, M. Cossi, J. M. Millam, M. Klene, C. Adamo, R. Cammi, J. W. Ochterski, R. L. Martin, K. Morokuma, O. Farkas, J. B. Foresman and D. J. Fox, *Gaussian* 16, Revision A.03, Gaussian, Inc., Wallingford CT, 2016.

